www.czasopisma.pan.pl PAN POLSKA AKADEMIA NAUK www.journals.pan.pl

Arch. Metall. Mater. **66** (2021), 1, 281-295

DOI: 10.24425/amm.2021.134786

JYRKI MIETTINEN[1], VILLE-VALTTERI VISURI[1*], TIMO FABRITIUS[1]

THERMODYNAMIC DESCRIPTION OF TERNARY Fe-B-X SYSTEMS. PART 8: Fe-B-Mo, WITH EXTENSION TO QUATERNARY Fe-B-Cr-Mo SYSTEM

Thermodynamic optimizations of the ternary Fe-B-Mo system and its binary sub-system B-Mo are presented. The Fe-B-Mo description is then extended to the quaternary Fe-B-Cr-Mo system by assessing the ternary B-Cr-Mo system. The thermodynamic descriptions of the other binaries (Fe-B, Fe-Cr, Fe-Mo, B-Cr, and Cr-Mo) and the other ternaries (Fe-B-Cr and Fe-Cr-Mo) are taken from earlier studies. In this study, the adjustable parameters of the B-Mo, Fe-B-Mo, and B-Cr-Mo systems were optimized using the experimental thermodynamic and the phase equilibrium data from the literature. The solution phases of the system (liquid, bcc and fcc) are described with the substitutional solution model, and most borides are treated as stoichiometric phases or semistoichiometric phases, using a simple two-sublattice model for the latter. The system's intermetallic phases, Chi, Mu, R, and Sigma (not dissolving boron) as well as boride M_3B_2, based on a formulation of $(Cr,Fe)(Cr,Fe,Mo)_2(B)_2$, are described with a three-sublattice model. Reasonable agreement is obtained between the calculated and measured phase equilibria in all four systems: B-Mo; Fe-B-Mo; B-Cr-Mo; and Fe-B-Cr-Mo.

Keywords: phase diagrams, thermodynamic modeling, thermodynamic database, Fe-based systems, Fe-B-X systems, Fe-B-Mo system, Fe-B-Cr-Mo system

1. Introduction

The present paper continues the previous study [1] related to the development of a boron containing iron-based Fe-B-X database. The previous contributions of Fe-B-Cr [1], Fe-B-Ni [2], Fe-B-Mn [3], Fe-B-V [4], Fe-B-Si [5], Fe-B-Ti [6], and Fe-B-C [7] are followed by a description for the ternary Fe-B-Mo and its extension to the quaternary Fe-B-Cr-Mo system, including the ternary B-Cr-Mo system. The aim is to obtain a simple and compatible thermodynamic database for iron-based alloys [8] that provides important and practical input data for the Interdendritic Solidification (IDS) software [9,10], which is a thermodynamic-kinetic tool for simulating the solidification of steels. Complex phase descriptions published in the literature are beyond the scope of this database, excluding, however, some intermetallic phases and carbides whose descriptions cannot be simplified. The Iron Alloys Database (IAD), which includes all the earlier assessed Fe-B-X descriptions [1-7], treats boron as a substitutional component to simplify calculations of the IDS software. Although it would be physically more correct way would be to treat it as an interstitial component, this simplifying assumption has virtually no effect on the calculated phase equilibria in this software. A similar simplification was made in the Fe-B description of Hallemans et al. [11] which our Fe-B-X descriptions are based on.

In this eighth part, thermodynamic descriptions of the B-Mo, Fe-B-Mo, B-Cr-Mo, and Fe-B-Cr-Mo systems are made using the experimental thermodynamic and phase equilibrium data from the literature. The binary thermodynamic parameters used in the quaternary Fe-B-Cr-Mo description are taken from [1,11] for Fe-B, [12,13] for Fe-Cr, [14-16] for Fe-Mo, [1,17] for B-Cr, and [16,18] for Cr-Mo, and the ternary parameters are taken from [1] for Fe-B-Cr and [16,18] for Fe-Cr-Mo.

The B-Mo system has been assessed by Spear and Wang [19], Yang and Chang [20], Yamada et al. [21] and Witusiewicz et al. [22]. The description of Witusiewicz et al. [22] is the most successful due to its systematic validation with a great number of experimental measurements and its realistic treatment of all borides as non-stoichiometric compounds. Nevertheless, as the IAD database favors simple compound descriptions and treats B as a substitutional element (in contrast to [22], in which B is treated as an interstitial element), one more B-Mo description is introduced in the present study. It combines the assessments by [19] and [20] introducing new description for the bcc, MoB_2,

[1] UNIVERSITY OF OULU, PROCESS METALLURGY RESEARCH UNIT, P.O. BOX 4300, FI-90014 UNIVERSITY OF OULU, FINLAND

* Corresponding author: ville-valtteri.visuri@oulu.fi

Mo_2B_5 and MoB_4 phases and treating all compounds as stoichiometric phases. The higher phase stabilities according to [20] were preferred to those by [21] due to their better usability in a later Fe-B-Mo description by Yang et al. [23] and this study.

The Fe-B-Mo system has been assessed successfully by Yang et al. [23], including their own measurements of liquid state phase equilibria and solid-state microstructures. Unfortunately, this description could not be adopted directly for the following three reasons. First, they apply interstitial filling of B atoms in the bcc and fcc phases instead of our substitutional filling [1]. The latter treatment is physically not as correct but cannot be changed, as already applied in the seven earlier descriptions of our Fe-B-X database. Second, the present descriptions for the liquid phase of the Fe-Mo and Cr-Mo systems, and the FeB phase of the Fe-B system, fixed in earlier studies [1,15,16], differ from those of [23]. A third reason is the present treatment of boride M_3B_2 with a three sublattice model as suggested by Pan [24]. This makes it easily extendable to the Fe-B-Cr-Mo system, with a formulation of $(Cr,Fe)(Cr,Fe,Mo)_2(B)_2$, whereas Yang et al. [23] treated that phase as a simple stoichiometric phase, $FeMo_2B_2$. Of course, that phase can later also be extended to respond to the compositional changes, but in this study, it was found better to make the optimization for the $(Cr,Fe)(Cr,Fe,Mo)_2(B)_2$ phase within the framework of the entire Fe-B-Cr-Mo system, not primarily for the Fe-B-Mo system alone. It is also noteworthy that the B-rich ternary boride assessed by Yang et al. [23] with formulation $(Fe,Mo)_{29}Mo_{15}B_{56}$ is not considered in the present study, because that phase does not participate in the solid-state phase equilibria of the Fe-Mo side of the system. Another ternary boride, labelled as τ_1-$Fe_{13}Mo_2B_5$ by Haschke et al. [25] and $(Fe_xMo_{1-x})_3B$ by Leithe-Jasper et al. [26] was treated as $Fe_{14}MoB_5$ by Yang et al. [23]. As this phase is stable in a narrow temperature range [23, 25], it was reasonable to treat it in the same way as proposed by Yang et al. [23], i.e. by keeping its stability sufficiently low to satisfy their DTA measurements.

The B-Cr-Mo system has been assessed professionally by Tojo et al. [27]. It provides detailed crystallographic descriptions of the borides, as well as the first-principle calculations made for some of them. However, as its binary Cr-B, Cr-Mo, and B-Mo data differ from those of the present database, this ternary system had to be reassessed to fit with the present Fe-B-Mo description for obtaining a compatible Fe-B-Cr-Mo description. It is noteworthy that Tojo et al. [27] treated the M_3B_2 boride as a two sublattice phase with a formulation of $(Cr,Mo)_3B_2$. This may be a better choice than the corresponding formulation of $(Cr)_1(Cr,Mo)_2B_2$ applied by Pan [24] and in this study. Nevertheless, as the three-sublattice model of Pan [24] worked well in describing the M_3B_2 phase, not only in the quaternary Fe-B-Cr-Mo system but in its quinary extension with Ni, it was accepted in the present Fe-B-X database.

2. Phases, modeling and data

Table 1 shows the phases and their modeling in the current Fe-B-Cr-Mo assessment. The solution phases of the system (liq-

TABLE 1

Phases and their modeling in the Fe-B-Cr-Mo description

Phase	Modeling
liquid (≈L)	(B,Cr,Fe,Mo), substitutional, RKM
bcc_A2 (≈bcc)	(B,Cr,Fe,Mo), substitutional, RKM
fcc_A1 (≈fcc)	(B,Cr,Fe,Mo), substitutional, RKM
Chi (≈χ)	$(Cr,Fe)_{24}(Cr,Mo)_{10}(Cr,Fe,Mo)_{24}$, sublattice, RKM
Mu (≈μ)	$(Cr,Fe)_7(Mo)_2(Cr,Fe,Mo)_4$, sublattice, RKM
R	$(Cr,Fe)_{27}(Mo)_{14}(Cr,Fe,Mo)_{12}$, sublattice, RKM
Sigma (≈σ)	$(Fe)_8(Cr,Mo)_4(Cr,Fe,Mo)_{18}$, sublattice, RKM
Fe_2Mo (≈λ, dissolving Cr)	$(Cr,Fe)_2(Mo)$, sublattice, RKM
Fe_2B (dissolving Cr and Mo)	$(Cr,Fe,Mo)_2(B)$, sublattice, RKM
FeB (dissolving Cr and Mo)	(Cr,Fe,Mo)(B), sublattice, RKM
Cr_2B (dissolving Fe and Mo)	$(Cr,Fe,Mo)_2(B)$, sublattice, RKM
Cr_5B_3 (dissolving Fe and Mo)	$(Cr,Fe,Mo)_5(B)_3$, sublattice, RKM
CrB (dissolving Fe and Mo)	(Cr,Fe,Mo)(B), sublattice, RKM
Cr_3B_4 (dissolving Mo)	$(Cr,Mo)_3(B)_4$, sublattice, RKM
CrB_2 (dissolving Mo)	$(Cr,Mo)(B)_2$, sublattice, RKM
CrB_4	$(Cr)(B)_4$, stoichiometric
Mo_2B (dissolving Cr)	$(Cr,Mo)_2(B)$, sublattice, RKM
MoB (dissolving Fe)	(Fe,Mo)(B), sublattice, RKM
MoB_2	$(Mo)_{3.77}(B)_{6.23}$, stoichiometric
Mo_2B_5	$(Mo)_{3.17}(B)_{6.83}$, stoichiometric
MoB_4	$(Mo)_{2.08}(B)_{7.92}$, stoichiometric
$Fe_{14}MoB_5$ (≈τ_1)	$(Fe)_{14}(Mo)_1(B)_5$, stoichiometric
M_3B_2 (≈τ_2)	$(Cr,Fe)(Cr,Fe,Mo)_2(B)_2$, sublattice, RKM
beta-rhombo-B (≈bet)	pure B

RKM = Redlich-Kister-Muggianu (excess model)

uid, bcc, and fcc) are described using the substitutional solution model, and most borides are treated as stoichiometric or semi-stoichiometric phases, using a simple two-sublattice model for the latter. A semistoichiometric boride is a two-sublattice phase, where metal atoms occupy the other sublattice and the boron atoms occupy the other one. As an example, see the modeling (formulation) of boride Fe_2B shown in Table 1. The intermetallic phases of the system, Chi, Mu, R, and Sigma, without dissolving boron, are described with a three-sublattice model applied in earlier studies of the Fe-Cr-Mo system. That same model is also applied for boride M_3B_2, appearing in the Fe-B-Mo, B-Cr-Mo, and Fe-B-Cr-Mo systems. No solubility of Fe, Cr, or Mo in the rhombohedral boron phase (referred to as "bet" below) is considered. Detailed descriptions of the substitutional solution and sublattice models and their parameters are available in Lukas et al. [28].

Table 2 shows the experimental and assessed information selected in the current optimization for the B-Mo, Fe-B-Mo, B-Cr-Mo, and Fe-B-Cr-Mo systems [19-21,26,29-48]. This information is essentially the same as applied in their earlier descriptions of [20-24,27].

3. Results

The thermodynamic description of the Fe-B-Cr-Mo system is shown in Table 3. The parameters marked with a reference code were taken from the earlier assessments [1,11-20], and the rest were optimized (*O) using the experimental data in Table 2. The Gibbs energy data for the pure components are taken from the compilations published by Dinsdale [49] and Ansara et al. [50].

TABLE 2

Experimental and assessed data applied in the assessment verification for the Fe-B-Mo system

System	Experimental data	Reference
B-Mo	Phase equilibria of the phase diagram	[29-34]
	Activity of B in solid alloys at 1,800 and 1,517°C	[30]
	Gibbs energy for the formation of solid alloys, at 1,800°C	[19,30,31,35,36]
	Enthalpy of formation of solid alloys at, 25°C	[19, 21, 35-38]
	Gibbs energy for the formation of borides	[19, 30, 39-41]
	Heat content of borides	[42, 43]
B-Fe-Mo	Primary liquid surfaces	[20]
	Four vertical sections, at 80, 75, 70, and 65 at-%Fe	[20]
	One vertical section, at 3.5 wt-%B	[20]
	Two isothermal sections at 1,050°C and 1,000°C	[26,44]
B-Cr-Mo	One isothermal section at 1,400°C	[45]
	One Mo-rich vertical section, at $w_B = w_{Cr}$	[46]
	Enthalpies of formation of CrB, Cr_3B_4 and M_3B_2, at 25°C	[27] FPC
Fe-B-Cr-Mo	Phase compositions in three iron-rich alloys at 1,000°C	[47,48]

w_i = weight fraction of solute i; FPC = first-principle calculations

TABLE 3

Thermodynamic description of the Fe-B-Cr-Mo system. Gibbs energy data for pure Fe, Cr, and Mo are given by Dinsdale [48]; for pure B, by Ansara et al. [49]. Parameter values except for Tc and b are in J/mol at

liquid (1 sublattice, sites: 1, constituents: B,Cr,Fe,Mo)	Ref.
$L^L_{B,Cr} = (-134{,}482 + 26.8T) + (+14{,}347)(x_B - x_{Cr}) + (-1{,}674)(x_B - x_{Cr})^2 + (-43{,}361)(x_B - x_{Cr})^3$	[17]
$L^L_{B,Fe} = (-133{,}438 + 33.946T) + (+ 7{,}771)(x_B - x_{Fe}) + (+29{,}739)(x_B - x_{Fe})^2$	[11]
$L^L_{B,Mo} = (-148{,}828 + 10.9T) + (-17{,}793)(x_B - x_{Mo}) + (+21{,}053)(x_B - x_{Mo})^2$	[20]
$L^L_{Cr,Fe} = (-17{,}737 + 7.997T) + (-1{,}331)(x_{Cr} - x_{Fe})$	[13]
$L^L_{Cr,Mo} = (+15{,}810 - 6.714T) + (-9{,}220)(x_{Cr} - x_{Mo})$	[16]
$L^L_{Fe,Mo} = (-6{,}900 - 0.23T) + (-9{,}000 + 3.85T)(x_{Fe} - x_{Mo})$	[15,16]
$L^L_{B,Cr,Fe} = (-90{,}000 - 20T)x_B + (-60{,}000 - 20T)x_{Cr} + (120{,}000 - 20T)x_{Fe}$	[1]
$L^L_{B,Fe,Mo} = (-50{,}000)x_B + (-120{,}000 - 50T)x_{Fe} + (-40{,}000)x_{Mo}$	*O
$L^L_{Cr,Fe,Mo} = (-10{,}000)x_{Cr} + (0)x_{Fe} + (-99{,}000)x_{Mo}$	[16]
bcc (1 sublattice, sites: 1, constituents: B,Cr,Fe,Mo)	**Ref.**
${}^oG^{bcc}_B = {}^oG^{bet}_B + (+43{,}514 - 12.217T)$	[49]
$L^{bcc}_{B,Cr} = (-37{,}000)$	[1]
$L^{bcc}_{B,Fe} = (-50{,}000 + 42T)$	[1]
$L^{bcc}_{B,Mo} = (-131{,}000 + 47T)$	*O
$L^{bcc}_{Cr,Fe} = (+20{,}500 - 9.68T)$	[12]
$L^{bcc}_{Cr,Mo} = (+28{,}890 - 7.962T) + (+5{,}974 - 2.428T)(x_{Cr} - x_{Mo})$	[18]

TABLE 2. Continued

$L^{bcc}_{Fe,Mo} = (+36{,}818 - 9.141T) + (-362 - 5.724T)(x_{Fe} - x_{Mo})$	[14]
$L^{bcc}_{Cr,Fe,Mo} = (+15{,}000 - 12T)$	[16]
$Tc^{bcc} = 1043x_{Fe} - 311x_{Cr} + x_{Fe}x_{Cr}(1{,}650 - 550(x_{Fe} - x_{Cr})) + x_{Fe}x_{Mo}(335 + 526(x_{Fe} - x_{Mo}))$	[18]
$\beta^{bcc} = 2.22x_{Fe} - 0.008x_{Cr} - 0.85x_{Fe}x_{Cr}$	[18]
fcc (1 sublattice, sites: 1, constituents: B,Cr,Fe,Mo)	**Ref.**
$^{o}G^{fcc}_{B} = {}^{o}G^{bet}_{B} + (+50{,}208 - 13.478T)$	[49]
$L^{fcc}_{B,Cr} = L^{bcc}_{B,Cr}$	[1]
$L^{fcc}_{B,Fe} = (-66{,}000 + 50T)$	[1]
$L^{fcc}_{B,Mo} = L^{bcc}_{B,Mo}$	*O
$L^{fcc}_{Cr,Fe} = (+10{,}833 - 7.477T) + (+1{,}410)(x_{Cr} - x_{Fe})$	[12]
$L^{fcc}_{Cr,Mo} = L^{bcc}_{Cr,Mo}$	[16]
$L^{fcc}_{Fe,Mo} = (+28{,}347 - 17.691T)$	[14]
$Tc^{fcc} = -201x_{Fe} - 1{,}109x_{Cr}$	[18]
$\beta^{fcc} = -2.1x_{Fe} - 2.46x_{Cr}$	[18]
Chi(χ) (3 sublattices, sites: 24:10:24, constituents: Cr,Fe:Cr,Mo:Cr,Fe,Mo)	**Ref.**
$^{o}G^{\chi}_{Cr:Cr:Cr} = 48{}^{o}G^{fcc}_{Cr} + 10{}^{o}G^{bcc}_{Cr} + (+109{,}000 + 123T)$	[18]
$^{o}G^{\chi}_{Cr:Cr:Fe} = 24{}^{o}G^{fcc}_{Cr} + 10{}^{o}G^{bcc}_{Cr} + 24{}^{o}G^{fcc}_{Fe} + (+500{,}000)$	[18]
$^{o}G^{\chi}_{Cr:Cr:Mo} = 24{}^{o}G^{fcc}_{Cr} + 10{}^{o}G^{bcc}_{Cr} + 24{}^{o}G^{fcc}_{Mo} + (+500{,}000)$	[18]
$^{o}G^{\chi}_{Cr:Mo:Cr} = 24{}^{o}G^{fcc}_{Cr} + 10{}^{o}G^{bcc}_{Mo} + 24{}^{o}G^{fcc}_{Cr} + (-26{,}000)$	[18]
$^{o}G^{\chi}_{Cr:Mo:Fe} = 24{}^{o}G^{fcc}_{Cr} + 10{}^{o}G^{bcc}_{Mo} + 24{}^{o}G^{fcc}_{Fe} + (+500{,}000)$	[18]
$^{o}G^{\chi}_{Cr:Mo:Mo} = 24{}^{o}G^{fcc}_{Cr} + 10{}^{o}G^{bcc}_{Mo} + 24{}^{o}G^{fcc}_{Mo} + (+500{,}000)$	[18]
$^{o}G^{\chi}_{Fe:Cr:Cr} = 24{}^{o}G^{fcc}_{Fe} + 10{}^{o}G^{bcc}_{Cr} + 24{}^{o}G^{fcc}_{Cr} + (+18{,}300 - 100T)$	[18]
$^{o}G^{\chi}_{Fe:Cr:Fe} = 48{}^{o}G^{fcc}_{Fe} + 10{}^{o}G^{bcc}_{Cr} + (+\ 7{,}300 - 100T)$	[18]
$^{o}G^{\chi}_{Fe:Cr:Mo} = 24{}^{o}G^{fcc}_{Fe} + 10{}^{o}G^{bcc}_{Cr} + 24{}^{o}G^{fcc}_{Mo} + (+100{,}000)$	[18]
$^{o}G^{\chi}_{Fe:Mo:Cr} = 24{}^{o}G^{fcc}_{Fe} + 10{}^{o}G^{bcc}_{Mo} + 24{}^{o}G^{fcc}_{Cr} + (+5{,}000 - 365T)$	[16]
$^{o}G^{\chi}_{Fe:Mo:Fe} = 48{}^{o}G^{fcc}_{Fe} + 10{}^{o}G^{bcc}_{rMo} + (+305{,}210 - 270T)$	[18]
$^{o}G^{\chi}_{Fe:Mo:Mo} = 24{}^{o}G^{fcc}_{Fe} + 10{}^{o}G^{bcc}_{Mo} + 24{}^{o}G^{fcc}_{Mo} + (+97{,}300 - 100T)$	[18]
Mu(μ) (3 sublattices, sites: 7:2:4, constituents: Cr,Fe:Mo:Cr,Fe,Mo)	**Ref.**
$^{o}G^{\mu}_{Cr:Mo:Cr} = 7{}^{o}G^{fcc}_{Cr} + 2{}^{o}G^{bcc}_{Mo} + 4{}^{o}G^{bcc}_{Cr} + (+130{,}000 - 100T)$	[18]
$^{o}G^{\mu}_{Cr:Mo:Fe} = 7{}^{o}G^{fcc}_{Cr} + 2{}^{o}G^{bcc}_{Mo} + 4{}^{o}G^{bcc}_{Fe} + (+130{,}000 - 100T)$	[18]
$^{o}G^{\mu}_{Cr:Mo:Mo} = 7{}^{o}G^{fcc}_{Cr} + 6{}^{o}G^{bcc}_{Mo} + (+130{,}000 - 100T)$	[18]
$^{o}G^{\mu}_{Fe:Mo:Cr} = 7{}^{o}G^{fcc}_{Fe} + 2{}^{o}G^{bcc}_{Mo} + 4{}^{o}G^{bcc}_{Cr} + (+130{,}000 - 100T)$	[18]
$^{o}G^{\mu}_{Fe:Mo:Fe} = 7{}^{o}G^{fcc}_{Fe} + 2{}^{o}G^{bcc}_{Mo} + 4{}^{o}G^{bcc}_{Fe} + (+39{,}475 - 6.032T)$	[14]
$^{o}G^{\mu}_{Fe:Mo:Mo} = 7{}^{o}G^{fcc}_{Fe} + 6{}^{o}G^{bcc}_{Mo} + (-46{,}663 - 5.891T)$	[14]
$L^{\mu}_{Cr,Fe:Mo:Mo} = (-45{,}000)$	[18]
R (3 sublattices, sites: 27:14:12, constituents: Cr,Fe:Mo:Cr,Fe,Mo)	**Ref.**
$^{o}G^{R}_{Cr:Mo:Cr} = 27{}^{o}G^{fcc}_{Cr} + 14{}^{o}G^{bcc}_{Mo} + 12{}^{o}G^{bcc}_{Cr} + (-20{,}000)$	[18]
$^{o}G^{R}_{Cr:Mo:Fe} = 27{}^{o}G^{fcc}_{Cr} + 14{}^{o}G^{bcc}_{Mo} + 12{}^{o}G^{bcc}_{Fe} + (+618{,}000 - 600T)$	[16]
$^{o}G^{R}_{Cr:Mo:Mo} = 27{}^{o}G^{fcc}_{Cr} + 26{}^{o}G^{bcc}_{Mo} + (-20{,}000)$	[18]
$^{o}G^{R}_{Fe:Mo:Cr} = 27{}^{o}G^{fcc}_{Fe} + 14{}^{o}G^{bcc}_{Mo} + 12{}^{o}G^{bcc}_{Cr} + (+573{,}000 - 600T)$	[16]
$^{o}G^{R}_{Fe:Mo:Fe} = 27{}^{o}G^{fcc}_{Fe} + 14{}^{o}G^{bcc}_{Mo} + 12{}^{o}G^{bcc}_{Fe} + (-77{,}487 - 50.486T)$	[14]
$^{o}G^{R}_{Fe:Mo:Mo} = 27{}^{o}G^{fcc}_{Fe} + 26{}^{o}G^{bcc}_{Mo} + (+313{,}474 - 289.472T)$	[14]
Sigma(σ) (3 sublattices, sites: 8:4:18, constituents: Fe:Cr,Mo:Cr,Fe,Mo)	**Ref.**
$^{o}G^{\sigma}_{Fe:Cr:Cr} = 8{}^{o}G^{fcc}_{Fe} + 22{}^{o}G^{bcc}_{Cr} + (+92{,}300 - 95.96T)$	[12]
$^{o}G^{\sigma}_{Fe:Cr:Fe} = 8{}^{o}G^{fcc}_{Fe} + 4{}^{o}G^{bcc}_{Cr} + 18{}^{o}G^{bcc}_{Fe} + (+117{,}300 - 95.96T)$	[12]
$^{o}G^{\sigma}_{Fe:Cr:Mo} = 8{}^{o}G^{fcc}_{Fe} + 4{}^{o}G^{bcc}_{Cr} + 18{}^{o}G^{bcc}_{Mo} + (+285{,}000 - 240T)$	[18]
$^{o}G^{\sigma}_{Fe:Mo:Cr} = 8{}^{o}G^{fcc}_{Fe} + 4{}^{o}G^{bcc}_{Mo} + 18{}^{o}G^{bcc}_{Cr} + (+460{,}000 - 340T)$	[18]
$^{o}G^{\sigma}_{Fe:Mo:Fe} = 8{}^{o}G^{fcc}_{Fe} + 4{}^{o}G^{bcc}_{Mo} + 18{}^{o}G^{bcc}_{Fe} + (-1{,}813 - 27.272T)$	[14]
$^{o}G^{\sigma}_{Fe:Mo:Mo} = 8{}^{o}G^{fcc}_{Fe} + 22{}^{o}G^{bcc}_{Mo} + (+83{,}326 - 69.618T)$	[14]
$L^{\sigma}_{Fe:Cr:Cr,Mo} = (-148{,}000)$	[18]
$L^{\sigma}_{Fe:Cr:Fe,Mo} = (+570{,}000)$	[18]
$L^{\sigma}_{Fe:Mo:Cr,Mo} = (+121{,}000)$	[18]
$L^{\sigma}_{Fe:Mo:Fe,Mo} = (+222{,}909)$	[14]
Fe_2Mo(λ) (2 sublattices, sites: 2:1, constituents: Cr,Fe:Mo)	**Ref.**
$^{o}G^{\lambda}_{Fe:Mo} = 2{}^{o}G^{fcc}_{Fe} + {}^{o}G^{bcc}_{Mo} + (-10{,}798 - 0.132T)$	[16]
$^{o}G^{\lambda}_{Cr:Mo} = 2{}^{o}G^{bcc}_{Cr} + {}^{o}G^{bcc}_{Mo}$	[16]

TABLE 2. Continued

Fe_2B (2 sublattices, sites: 2:1, constituents: Cr,Fe,Mo:B)	**Ref.**
${}^{o}G^{Fe2B}_{Cr:B} = 2{}^{o}G^{bcc}_{Cr} + {}^{o}G^{bet}_{B} + (-18{,}000 + 15T)$	[1]
${}^{o}G^{Fe2B}_{Fe:B} = 2{}^{o}G^{bcc}_{Fe} + {}^{o}G^{bet}_{B} + (-78{,}783 + 10.398T)$	[11]
${}^{o}G^{Fe2B}_{Mo:B} = 2{}^{o}G^{bcc}_{Mo} + {}^{o}G^{bet}_{B}$	*O
$L^{Fe2B}_{Cr,Fe:B} = (-126{,}000)$	[1]
$L^{Fe2B}_{Fe,Mo:B} = (-60{,}000)$	*O
FeB (2 sublattices, sites: 1:1, constituents: Cr,Fe,Mo:B)	**Ref.**
${}^{o}G^{FeB}_{Cr:B} = {}^{o}G^{bcc}_{Cr} + {}^{o}G^{bet}_{B} + (-20{,}000 + 10T)$	[1]
${}^{o}G^{FeB}_{Fe:B} = {}^{o}G^{bcc}_{Fe} + {}^{o}G^{bet}_{B} + (-70{,}300 + 12T)$	[1]
${}^{o}G^{FeB}_{Mo:B} = {}^{o}G^{bcc}_{Mo} + {}^{o}G^{bet}_{B}$	*O
$L^{FeB}_{Cr,Fe:B} = (-90{,}000)$	[1]
$L^{FeB}_{Fe,Mo:B} = (-60{,}000 - 30T)$	*O
Cr_2B (2 sublattices, sites: 2:1, constituents: Cr,Fe,Mo:B)	**Ref.**
${}^{o}G^{Cr2B}_{Cr:B} = 2{}^{o}G^{bcc}_{Cr} + {}^{o}G^{bet}_{B} + (-92{,}544 + 4.44T)$	[17]
${}^{o}G^{Cr2B}_{Fe:B} = 2{}^{o}G^{bcc}_{Fe} + {}^{o}G^{bet}_{B} + (-18{,}000 + 15T)$	[1]
${}^{o}G^{Cr2B}_{Mo:B} = 2{}^{o}G^{bcc}_{Mo} + {}^{o}G^{bet}_{B} + (-90{,}000)$	*O
$L^{Cr2B}_{Cr,Fe:B} = (-255{,}000 + 60T)$	[1]
$L^{Cr2B}_{Cr,Mo:B} = (-45{,}000) + (-36{,}000)(y_{Cr} - y_{Mo})$	*O
$L^{Cr2B}_{Cr,Fe,Mo:B} = (+51{,}000)$	*O
Cr_5B_3 (2 sublattices, sites: 5:3, constituents: Cr,Fe,Mo:B)	**Ref.**
${}^{o}G^{Cr5B3}_{Cr:B} = 5{}^{o}G^{bcc}_{Cr} + 3{}^{o}G^{bet}_{B} + (-274{,}008 + 18.056T)$	[17]
${}^{o}G^{Cr5B3}_{Fe:B} = 5{}^{o}G^{bcc}_{Fe} + 3{}^{o}G^{bet}_{B}$	[1]
${}^{o}G^{Cr5B3}_{Mo:B} = 5{}^{o}G^{bcc}_{Mo} + 3{}^{o}G^{bet}_{B} + (-336{,}000 + 16T)$	*O
$L^{Cr5B3}_{Cr,Fe:B} = (-740{,}000 + 256T)$	[1]
$L^{Cr5B3}_{Cr,Mo:B} = (-248{,}000 + 32T)$	*O
CrB (2 sublattices, sites: 1:1, constituents: Cr,Fe,Mo:B)	**Ref.**
${}^{o}G^{CrB}_{Cr:B} = {}^{o}G^{bcc}_{Cr} + {}^{o}G^{bet}_{B} + (-80{,}000 + 6.48T)$	[1]
${}^{o}G^{CrB}_{Fe:B} = {}^{o}G^{bcc}_{Fe} + {}^{o}G^{bet}_{B} + (-20{,}000 + 10T)$	[1]
${}^{o}G^{CrB}_{Mo:B} = {}^{o}G^{bcc}_{Mo} + {}^{o}G^{bet}_{B} + (-101{,}400)$	*O
$L^{CrB}_{Cr,Fe:B} = (-120{,}000 + 40T) + (-80{,}000 + 40T)(y_{Cr} - y_{Fe})$	[1]
$L^{CrB}_{Cr,Mo:B} = (-7{,}000)$	*O
Cr_3B_4 (2 sublattices, sites: 3:4, constituents: Cr,Mo:B)	**Ref.**
${}^{o}G^{Cr3B4}_{Cr:B} = 3{}^{o}G^{bcc}_{Cr} + 4{}^{o}G^{bet}_{B} + (-300{,}888 + 34.65T)$	[17]
${}^{o}G^{Cr3B4}_{Mo:B} = 3{}^{o}G^{bcc}_{Mo} + 4{}^{o}G^{bet}_{B} + (-273{,}000)$	*O
$L^{Cr3B4}_{Cr,Mo:B} = (-98{,}000)$	*O
CrB_2 (2 sublattices, sites: 1:2, constituents: Cr,Mo:B)	**Ref.**
${}^{o}G^{CrB2}_{Cr:B} = {}^{o}G^{bcc}_{Cr} + 2{}^{o}G^{bet}_{B} + (-119{,}061 + 12.552T)$	[17]
${}^{o}G^{CrB2}_{Mo:B} = {}^{o}G^{bcc}_{Mo} + 2{}^{o}G^{bet}_{B} + (-90{,}000)$	*O
$L^{CrB2}_{Cr,Mo:B} = (-30{,}000)$	*O
CrB_4 (2 sublattices, sites: 1:4, constituents: Cr:B)	**Ref.**
${}^{o}G^{CrB4}_{Cr:B} = {}^{o}G^{bcc}_{Cr} + 4{}^{o}G^{bet}_{B} + (-124{,}750 + 15.75T)$	[1]
Mo_2B (2 sublattices, sites: 2:1, constituents: Cr,Mo:B)	**Ref.**
${}^{o}G^{Mo2B}_{Cr:B} = 2{}^{o}G^{bcc}_{Cr} + {}^{o}G^{bet}_{B} + (-90{,}000 + 4.5T)$	*O
${}^{o}G^{Mo2B}_{Mo:B} = 2{}^{o}G^{bcc}_{Mo} + {}^{o}G^{bet}_{B} + (-126{,}528 + 6T)$	[20]
$L^{Mo2B}_{Cr,Mo:B} = (-15{,}000) + (-54{,}000)(y_{Cr} - y_{Mo}) + (-15{,}000)(y_{Cr} - y_{Mo})^2$	*O
MoB (2 sublattices, sites: 1:1, constituents: Fe,Mo:B)	**Ref.**
${}^{o}G^{MoB}_{Fe:B} = {}^{o}G^{bcc}_{Fe} + {}^{o}G^{bet}_{B}$	*O
${}^{o}G^{MoB}_{Mo:B} = {}^{o}G^{bcc}_{Mo} + {}^{o}G^{bet}_{B} + (-104{,}034 + 0.42T)$	[20]
$L^{MoB}_{Fe,Mo:B} = (-70{,}000)$	*O
MoB_2 (2 sublattices, sites: 3.77:6.23, constituents: Mo:B)	**Ref.**
${}^{o}G^{MoB2}_{Mo:B} = 3.77{}^{o}G^{bcc}_{Mo} + 6.23{}^{o}G^{bet}_{B} + (-455{,}100 - 3.4T)$	*O
Mo_2B_5 (2 sublattices, sites: 3.17:6.83, constituents: Mo:B)	**Ref.**
${}^{o}G^{Mo2B5}_{Mo:B} = 3.17{}^{o}G^{bcc}_{Mo} + 6.83{}^{o}G^{bet}_{B} + (-511{,}200 + 43T)$	*O
MoB_4 (2 sublattices, sites: 2.08:7.92, constituents: Mo:B)	**Ref.**
${}^{o}G^{MoB4}_{Mo:B} = 2.08{}^{o}G^{bcc}_{Mo} + 7.92{}^{o}G^{bet}_{B} + (-341{,}220 + 31T)$	*O

TABLE 2. Continued

$Fe_{14}MoB_5$ (τ_1) (3 sublattices, sites: 14:1:5, constituents: Fe:Mo:B) ${}^oG^{\tau 1}_{Fe:Mo:B} = 14{}^oG^{bcc}_{Fe} + {}^oG^{bcc}_{Mo} + 5{}^oG^{bet}_{B} + (-423{,}800 + 30T)$	**Ref.** *O
M_3B_2 (τ_2) (3 sublattices, sites: 1:2:2, constituents: Cr,Fe:Cr,Fe,Mo:B) ${}^oG^{\tau 2}_{Cr:Cr:B} = 3{}^oG^{bcc}_{Cr} + 2{}^oG^{bet}_{B} + (-145{,}000 + 10T)$ ${}^oG^{\tau 2}_{Cr:Fe:B} = {}^oG^{bcc}_{Cr} + 2{}^oG^{bcc}_{Fe} + 2{}^oG^{bet}_{B} + (-200{,}000 + 35T)$ ${}^oG^{\tau 2}_{Cr:Mo:B} = {}^oG^{bcc}_{Cr} + 2{}^oG^{bcc}_{Mo} + 2{}^oG^{bet}_{B} + (-257{,}000 + 10T)$ ${}^oG^{\tau 2}_{Fe:Cr:B} = {}^oG^{bcc}_{Fe} + 2{}^oG^{bcc}_{Cr} + 2{}^oG^{bet}_{B} + (-238{,}000 + 35T)$ ${}^oG^{\tau 2}_{Fe:Fe:B} = 3{}^oG^{bcc}_{Fe} + 2{}^oG^{bet}_{B} + (-50{,}000 + 13T)$ ${}^oG^{\tau 2}_{Fe:Mo:B} = {}^oG^{bcc}_{Fe} + 2{}^oG^{bcc}_{Mo} + 2{}^oG^{bet}_{B} + (-262{,}000 + 13T)$ $L^{\tau 2}_{Cr:Cr,Mo:B} = (-82{,}000 + 10T)$	**Ref.** *O *O *O *O *O *O *O

*O – Parameter optimized in this study

The calculated results are compared with the original experimental data to verify the optimization. All calculations were carried out using the ThermoCalc software [51].

Figures 1 and 2 show the calculated phase diagrams of the binary systems of Fe-B [1] and Fe-Mo [15,16]. The agreement with the measured data of phase equilibria, activity, and enthalpy is reasonable, as shown in these assessments. This also concerns the binary assessments of Fe-Cr [13], B-Cr [1], and Cr-Mo [16], and the ternary assessments of Fe-Cr-B [1] and Fe-Cr-Mo [16].

For the remaining systems, Mo-B, Fe-B-Mo, Cr-Mo-B, and Fe-B-Cr-Mo, the calculated results, as well as their comparison with experimental data, are shown in the following subsections.

3.1. System B-Mo

Results of the present calculations are compared with the experimental data (Table 2) in Table 4 and Figures 3-9. The agreement is reasonably good. Figures 3 and 4 also show (by dotted lines) the phase equilibria calculated by Witusiewicz et al. [22]. In Figure 3, note the non-stoichiometric borides by [22], particularly for the MoB_2 and Mo_2B_5 phases, and the division of MoB to α-MoB and β-MoB borides, causing two additional three-phase equilibria in the phase diagram (at 2,180°C and 1,801°C). In the present study and that by Yang and Chang [20], instead, only one MoB phase is considered, which simplifies the calculations. Also note the calculated lower temperature for the reaction L = Mo_2B_5 + bet in regard to the temperature calculated by Yang and Chang [20] and assessed by Brewer and Lamoreaux [31] (see Figure 3 and Table 4). This originates in the decision to treat all Mo-B borides as simple stoichiometric phases and their Gibbs energy expressions as simple temperature functions.

As shown in Table 4, the measured B solubilities in the bcc exhibit a large scatter. A detailed analysis of the available measurements was carried out by Witusiewicz et al. [22] who assessed two solubility curves from the measurements by Zakharov at al. [34]. These are shown by the square symbols with numbers 1 and 2 in Figure 4. The lower solubility values following curve 1 were proposed to be more reliable than those following curve 2. Accordingly, the calculations by Witusiewicz et al. [22] agree

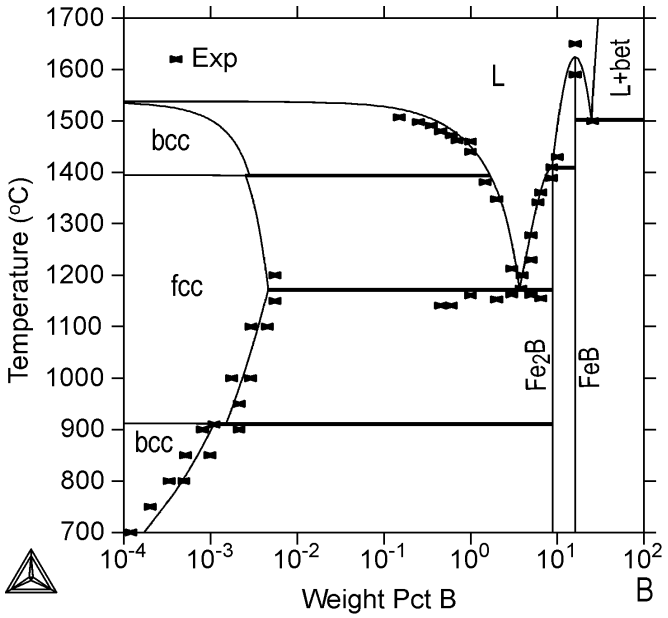

Fig. 1. Fe-B phase diagram calculated by Miettinen and Vassilev [1], with the experimental data points reviewed in [1]

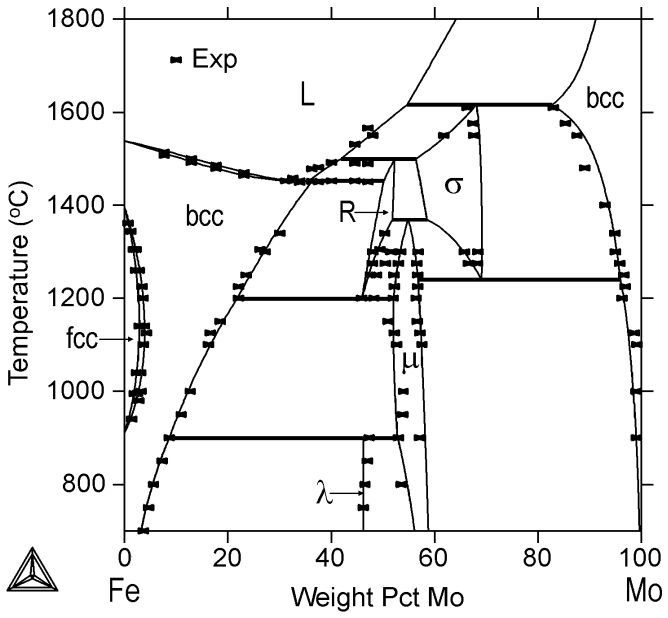

Fig. 2. Fe-Mo phase diagram calculated by Miettinen et al. [15,16], with the experimental data points reviewed in [15,16]

TABLE 4

Calculated (Calc.) and experimental (Exp.) invariant points of the B-Mo systems. C_B^{ϕ} denotes the composition of boron in phase ϕ

Reaction with phases $\phi1$, $\phi2$, $\phi3$	T (°C)	$C_B^{\phi1}$ (at%)	$C_B^{\phi2}$ (at%)	$C_B^{\phi3}$ (at%)	Reference
L = bcc + Mo_2B	2,177	20.4	0.46	33.33	Calc. This study
	2,176	20.3	0.21	33.33	Calc. [20]
	2,197	20.3	1.43	33.33	Calc. [21]
	2,178	21.7	0.40	32.60	Calc. [22]
	2,175	23	0.80	33	Exp. [31]
L + MoB = Mo_2B	2,276	29.77	50	33.33	Calc. This study
	2,280	30	49	34	Exp. [31]
L = MoB	2,600	50	50		Calc. This study
	2,600	50	50		Exp. [31]
L + MoB = MoB_2	2,376	65.64	50	62.3	Calc. This study
	2,375	70	52	63	Exp. [31]
MoB_2 = MoB + Mo_2B_5	1,516	62.3	50	68.3	Calc. This study
	1,517	62	50	67	Exp. [31]
L + MoB_2 = Mo_2B_5	2,137	78.76	62.3	68.3	Calc. This study
	2,140	79	62	68	Exp. [31]
L = Mo_2B_5 + bet	1,912	88.68	68.3	100	Calc. This study
	1,920	94	68	~98	Exp. [31]
Mo_2B_5 + bet = MoB_4	1,807	68.3	100	79.2	Calc. This study
	1,807	68	~99	79	Exp. [31]

well with curve 1. On the other hand, this contradicts with the maximum solubility of 0.91 wt% B assessed by Brewer and Lamoreaux [31] (see Table 4). The calculations of this study give slightly higher solubilities than curve 1 but clearly lower solubilities than curve 2. By making this choice, a good agreement was obtained between the calculated and experimental B solubilities in the Mo-rich bcc phase of the B-Cr-Mo system as demonstrated later in the text. Concerning the activity, enthalpy and Gibbs energy data in Figures 5-9, the agreement between the calculations and measurements is quite good, and comparable to that by Witusiewicz et al. [22]. These results reveal that the Gibbs energy expressions of the borides are well optimized in spite of their stoichiometric nature. In Figure 7 note the less negative values for the Gibbs energies of the formation of borides

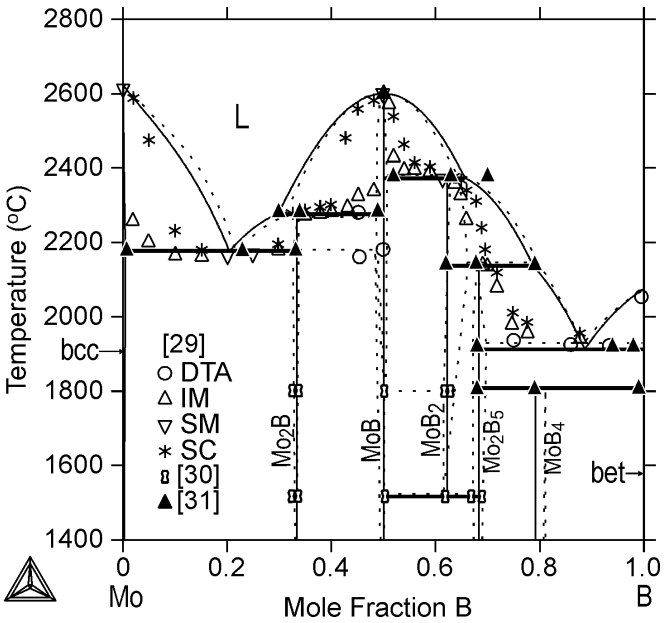

Fig. 3. The calculated B-Mo phase diagram, with the experimental data points by Rudy [29] and Storms and Müller [30] and those assessed by Brewer and Lamoreaux [31]. DTA = differential thermal analysis, IM = incipient melting, SM = sharp melting, and SC = specimen collapsed. The solid lines refer to the calculations of this study; the dotted lines refer to those by Witusiewicz et al. [22]

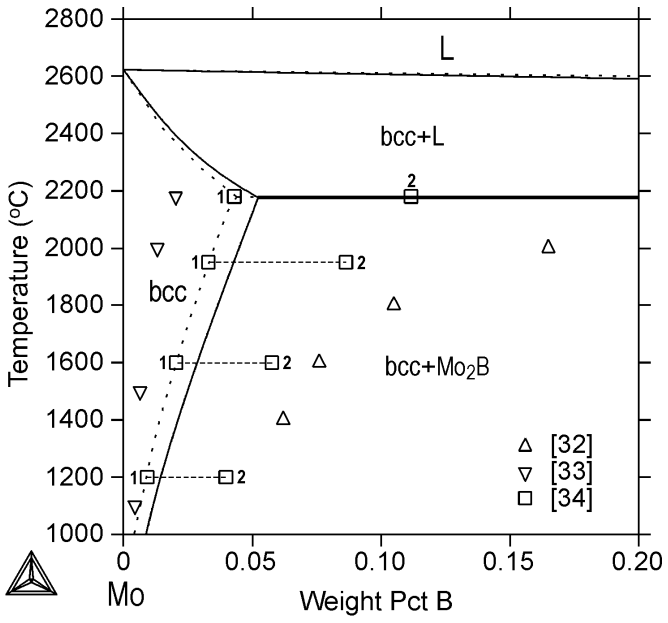

Fig. 4. The calculated Mo-rich part of the B-Mo phase diagram, with the experimental data points by Chuang et al. [32], Kharitonov et al. [33] and Zakharov et al. [34]. Two solubility curves indicated by square symbols 1 and 2 were assessed by Witusiewicz et al. [22] from the data by [34]. The solid lines refer to the calculations of this study; the dotted lines refer to those of Witusiewicz et al. [22]

obtained by Yamada et al. [21] using the first-principle calculations. These values agree well with their own thermodynamic assessment data, but at the same time, their invariant points for reaction L = bcc + Mo_2B do not agree as well with the assessed data points by [31] (see Table 4). Finally, the enthalpies of mixing liquid B-Mo alloys were calculated and compared with the assessed data by Franke and Neuschütz [36] at 2727°C. In this case, the agreement is worse than that obtained by Witusiewicz et al. [22], but better than that obtained by Yamada et al. [21]. For example, the calculated mixing enthalpy values at 50 at% were reported to be –30 kJ/mol in [21], –37.3 kJ/mol in this study and –45.5 kJ/mol in [22], whereas the assessed value is approximately –50 kJ/mol [36]. However, as the data by [36] represents an estimation rather than direct experimental data [22], no trials were made to re-optimize the liquid phase interaction parameters of the B-Mo system.

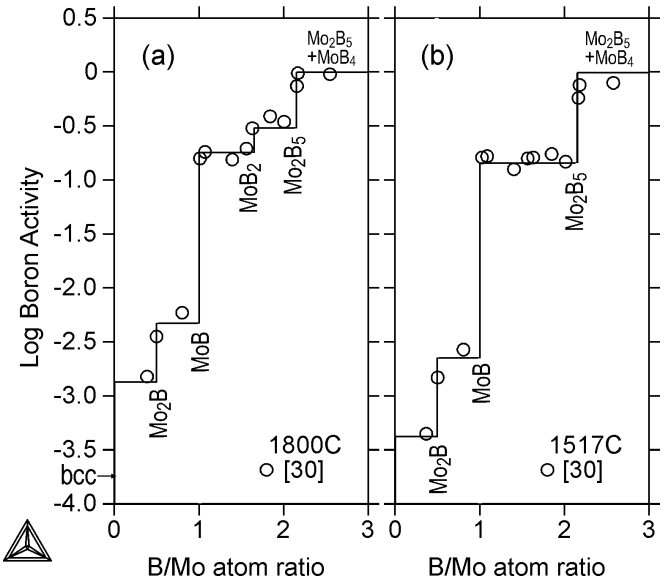

Fig. 5. The calculated B activity of solid B-Mo alloys at 1,800°C (a) and 1,517°C (b), with experimental data points by Storms and Müller [30]. The reference state used is pure beta-rhombo B

3.2. System Fe-B-Mo

The results of calculations (Table 2) are presented with the experimental data in Figures 10-19 and Table 5. The agreement is comparable to that obtained by Yang et al. [23]. Figure 10 shows that the calculated liquidus projection of the system fits well with the primary surfaces detected by Yang et al. [23]. The calculated invariant points of this study and Yang et al. [23] are in a reasonable accordance as well. The reaction L = fcc + Fe_2B + τ_2 (E_2) of the present calculations, however, is hypothetical. It appears only if the barely stable τ_1 phase cannot form, e.g. due to kinetic limitations in some real cooling process. Otherwise, a tiny primary surface region of the τ_1 phase is formed, with three new invariant points, P', U' and E' (see the magnification window in Figure 10 and the reactions of these invariant points in Table 5). Note that the appearance of the primary τ_1 surface is supported by one measurement of Yang et al. [23], suggesting the reaction L = τ_1 + fcc at 1140°C, but in spite of that, they did not allow the τ_1 phase to come stable with the presence of liquid. Consequently, the reaction L = fcc + Fe_2B + τ_2 (E_2) is not hypothetical according to their calculations. The stability region of the τ_1 phase was reported [23] to be 1110-1080°C, whereas that region by the present calculations is 1126-1090°C. Within

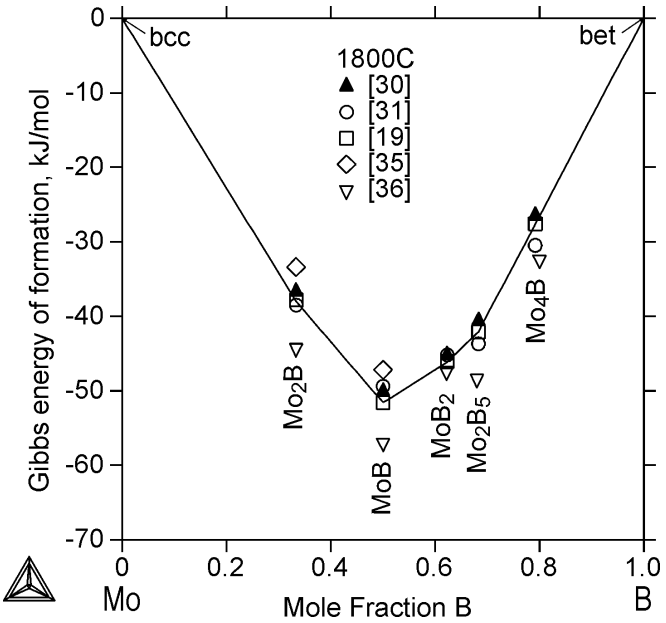

Fig. 6. The calculated Gibbs energy for the formation of solid B-Mo alloys at 1,800°C, with experimental data points by Storms and Müller [30] and Morishita et al. [35], as well as assessed data points by Spear and Wang [19], Brewer and Lamoreaux [31], and Franke and Neuschütz [36]. The reference states used are pure bcc Mo and pure beta-rhombo B

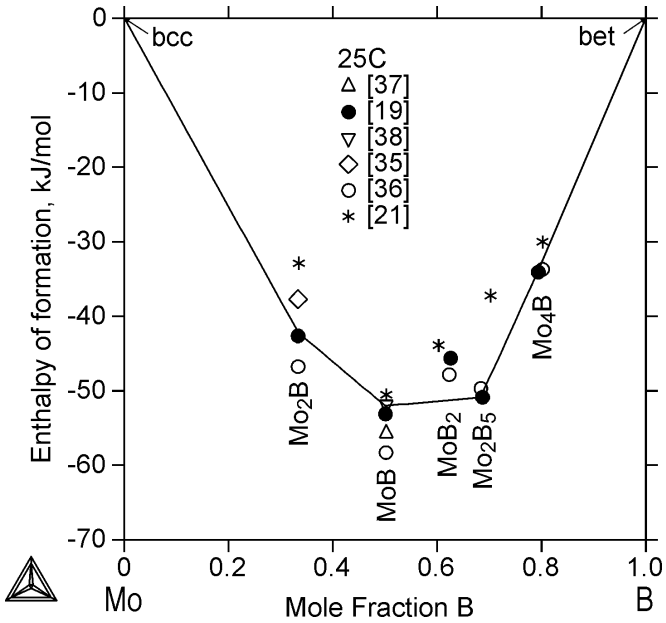

Fig. 7. The calculated enthalpy for the formation of solid Mo-B alloys at 25°C, with experimental data points of Morishita et al. [35], Maslov et al. [37] and Lavut et al. [38], as well as assessed data points by Spear and Wang [19], Yamada et al. [21] and Franke and Neuschütz [36]. The reference states used are pure bcc Mo and pure beta-rhombo B

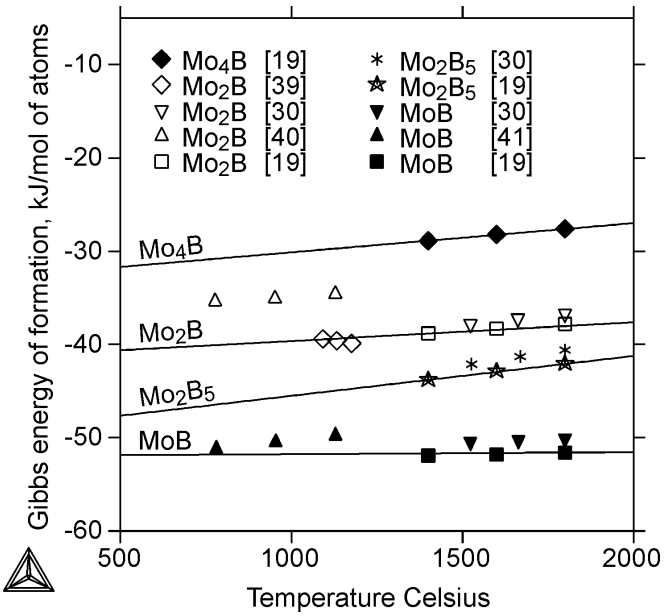

Fig. 8. The calculated Gibbs energies for the formation of borides Mo_2B, MoB and Mo_2B_5, with experimental data points by Storms and Müller [30], Baehren and Vollath [39] and Omori et al. [40, 41] in addition to the assessed data points by Spear and Wang [19]. The reference states used are pure bcc Mo and beta-rhombo B

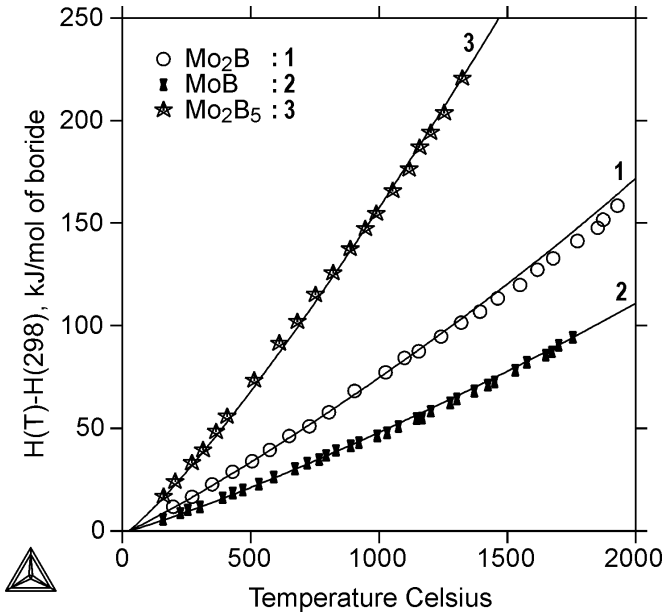

Fig. 9. The calculated heat content of borides Mo_2B, MoB and Mo_2B_5, with experimental data points by Serbova [42] and Bolgar et al. [43]

that region, liquid and τ_1 phases are simultaneously present in a narrow temperature interval of 1126-1124°C. In both calculations, the τ_1 phase stability was kept low to maintain a reasonable agreement between the calculations and the DTA measurements by Yang et al. [23].

The five calculated vertical sections in Figures 11-15 and the isothermal section of 1,200°C in Figure 16 agree reasonably well with the measurements of Yang et al. [23], though some deviation can also be seen, *e.g.* for some secondary arrests in Figure 12.

The isothermal sections of Figures 17 and 18 reveal that the bcc(Mo) + τ_2 equilibrium at 1,050°C changes to the μ + Mo_2B equilibrium at 1,000°C. This information was used to optimize the parameters for the Gibbs energy of formation of the M_3B_2 (τ_2) phase, i.e. ${}^{o}G^{\tau 2}_{Fe:Fe:B}$ and ${}^{o}G^{\tau 2}_{Fe:Mo:B}$. Another criterion was that an increase of temperature should destabilize the M_3B_2 phase as much as possible. This resulted in a temperature dependency of 13T for these two parameters. In Figures 16-18, the calculated near-stoichiometric composition (~$FeMo_2B_2$) for boride M_3B_2 (τ_2) is noteworthy. This has been confirmed by several researchers, as Raghavan [53] states, though a non-stoichiometric exten-

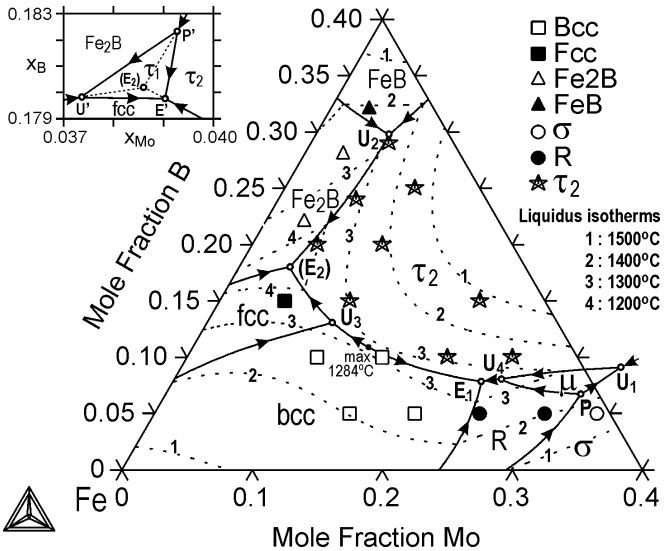

Fig. 10. Calculated liquidus projection in the Fe-rich corner of the Fe-B-Mo system, with experimental data points of Yang et al. [23]. The calculated liquidus isotherms between 1,500 and 1,200°C (dotted lines) are also shown. Invariant point E_2 becomes valid only by the absence of the barely stable τ_1 phase (see the magnification figure included)

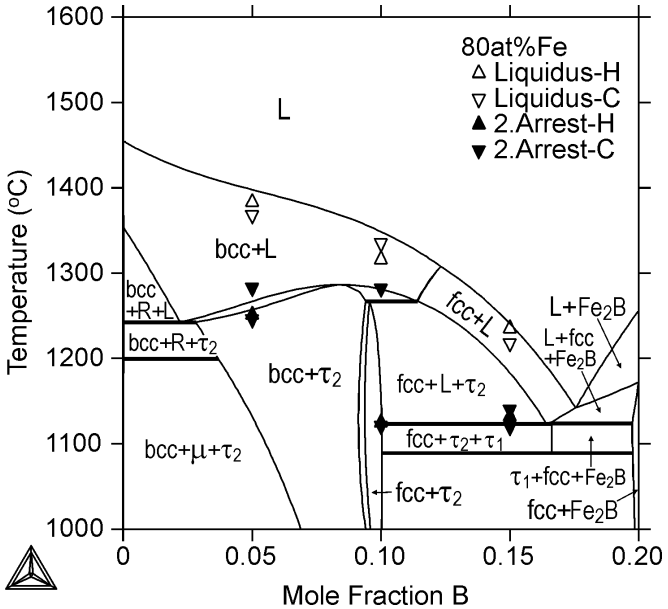

Fig. 11. Calculated vertical section at 80 at% Fe in the Fe-B-Mo system, with experimental data points of Yang et al. [23]. C denotes cooling; H denotes heating

TABLE 5

Calculated and experimental invariant points in the Fe-rich corner of the Fe-B-Mo system

Reaction	Type	T (°C)	at % Mo in liquid	at % B in liquid	Reference
L + R + s = μ	P	1,368 1,368	31.89 32.7	6.73 7.2	Calc. This study Calc. [23]
L + s = μ + τ_2	U_1	1,329 1,330	33.77 34.2	9.13 9.7	Calc. This study Calc. [23]
L + FeB = Fe_2B + τ_2	U_2	1,313 1,320	5.66 4.6	29.75 27.9	Calc. This study Calc. [23]
L + bcc = fcc + τ_2	U_3	1,267 1,241 1,250	9.65 8.1	13.09 14.3	Calc. This study Calc. [23] Exp. [23]
L + μ = R + τ_2	U_4	1,255 1,297	25.04 28.8	8.08 9.3	Calc. This study Calc. [23]
L = bcc + R + τ_2	E_1	1,244 1,257 1,255	23.72 23.9	7.86 8.6	Calc. This study Calc. [23] Exp. [23]
L = fcc + Fe_2B + τ_2*	E_2	1,122 1,138 1,122 1,132-1,092	3.86 3.7	18.02 17.8	Calc. This study Calc. [23] Exp. [23] Exp.[52]
L + Fe_2B + τ_2 = τ_1 L + Fe_2B = fcc + τ_1 L = fcc + τ + τ_1	P' U' E'	1,126.6 1,123.7 1,123.6	3.929 3.733 3.903	18.237 17.980 17.976	Calc. This study Calc. This study Calc. This study

*) Reaction L = fcc + Fe_2B + τ_2 of the present calculations is hypothetical. By the presence of the barely stable τ_1 phase, this reaction is replaced by the three new reactions shown at the bottom of this table. Correspondingly, invariant point E_2 is replaced with invariant points P', U' and E' shown in Figure 10.

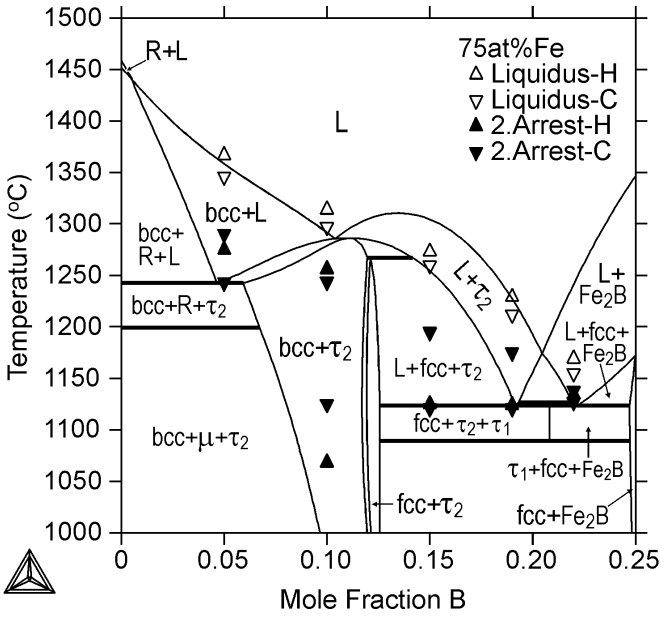

Fig. 12. Calculated vertical section at 75 at% Fe in the Fe-B-Mo system, with experimental data points of Yang et al. [23]. C denotes cooling; H denotes heating

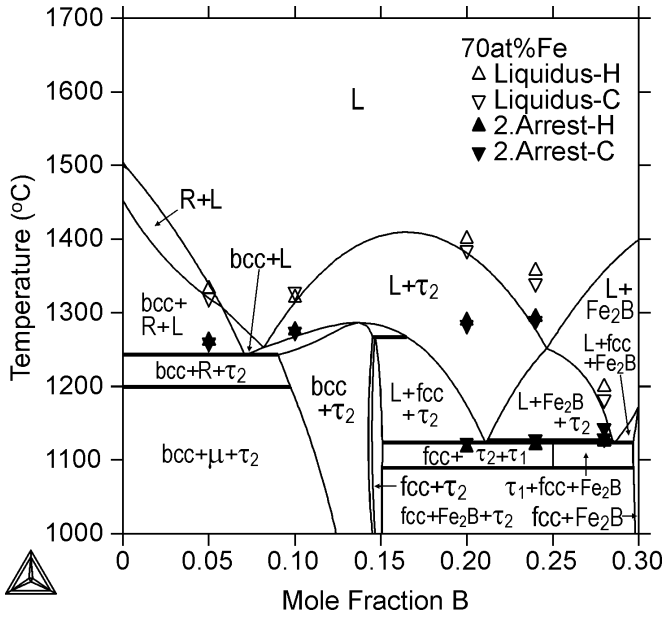

Fig. 13. Calculated vertical section at 70 at% Fe in the Fe-B-Mo system, with experimental data points of Yang et al. [23]. C denotes cooling; H denotes heating

sion of this phase, with 32-40at%Mo, has also been suggested [44], as shown in Figure 18.

Finally, Figure 19 shows the calculated solubility of B in the system's fcc and bcc phases. Increasing the Mo content promotes the formation of τ_2, which considerably decreases the B solubility in fcc and bcc. The B solubility is also decreased by a temperature decrease from 1,150 to 1,000°C.

3.3. System B-Cr-Mo

The results of calculations for the B-Cr-Mo system are presented in Figures 20-24, and Tables 6 and 7. The calculated liquidus projection of Figure 20 and the invariant points of Table 6 should be considered tentative due to the lack of experimental data for the liquid phase or its equilibria with

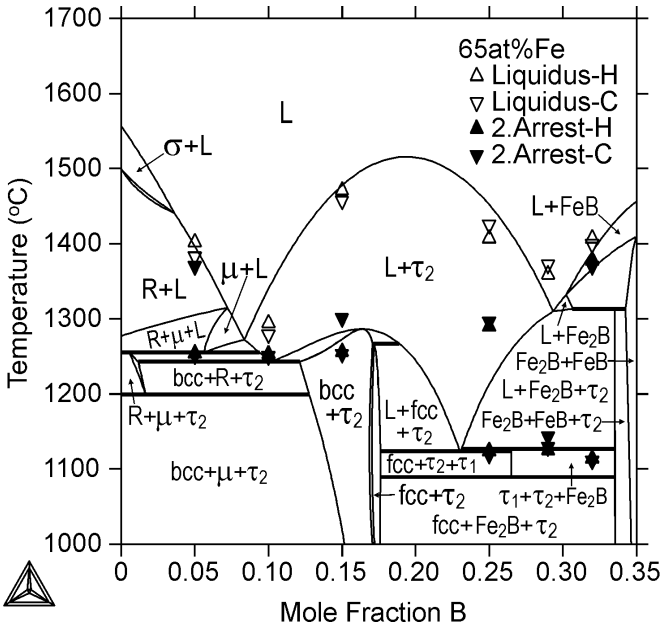

Fig. 14. Calculated vertical section at 65 at% Fe in the Fe-B-Mo system, with experimental data points of Yang et al. [23]. C denotes cooling; H denotes heating

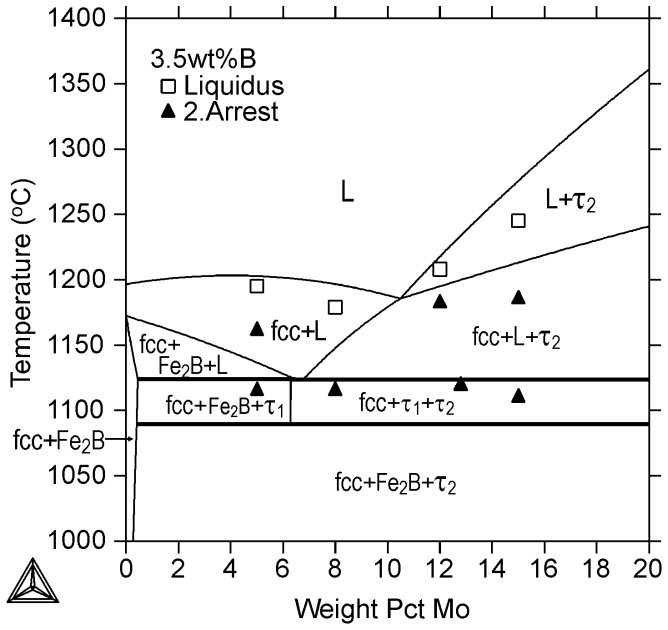

Fig. 15. Calculated vertical section at 3.5 wt% B in the Fe-B-Mo system, with experimental data points of Yang et al. [23]

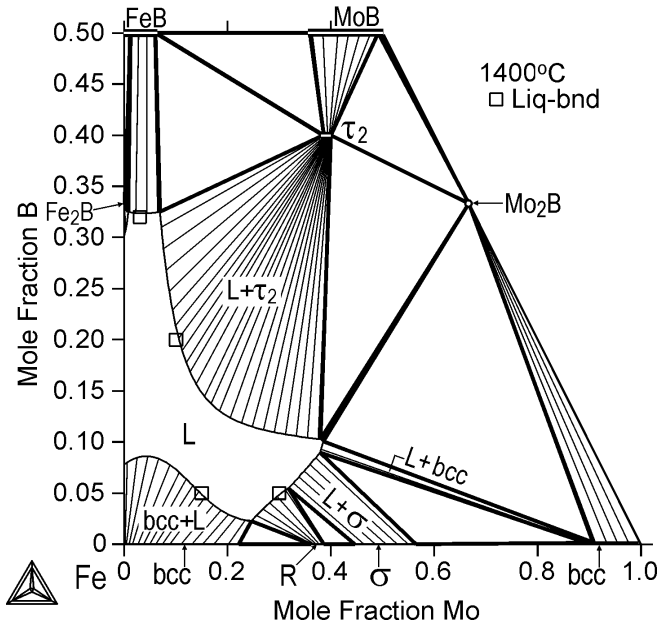

Fig. 16. Calculated isotherm of 1,400°C in the Fe-B-Mo system, with experimental data points of Yang et al. [23]. Abbreviation Liq-bnd denotes the liquid phase boundary

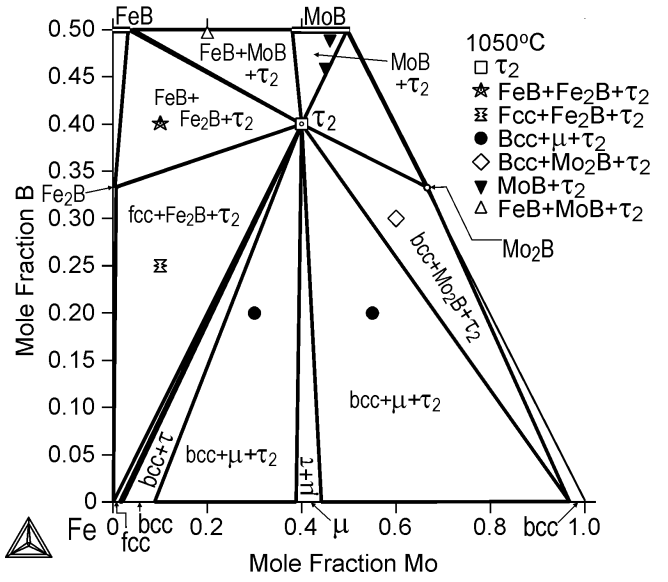

Fig. 17. Calculated isotherm of 1,050°C in the Fe-B-Mo system, with experimental data points of Leithe-Jasper et al. [26]

other phases. The present liquidus projection, which shows an extensive primary surface for boride Cr_5B_3, differs significantly from that of Tojo et al. [27], where the dominant boride, in the region of $0.15 < x_B < 0.35$, is Mo_2B. This discrepancy is due to their heavy emphasis on their own first-principle calculations on the enthalpies of formation of borides. Table 7 shows the corresponding agreement by the present calculations, which is reasonable, but worse that obtained by [27]. This is mainly due to the very different boride stabilities fixed in the earlier B-Cr description [1] before the paper by Tojo et al. [27]. However, the main reason for not adopting the boride expressions from [27] is their complex composition dependency (probably due to the first-principle calculations) and the poor adjustability of the two-sublattice treatment to describe the near-stoichiometric M_3B_2 phase of the Fe-Mo-B system. Instead, the three-sublattice treatment of Table 2 safely keeps the composition of M_3B_2very close to $FeMo_2B_2$ (as several researchers propose) but allows a clear compositional extension for this phase with Cr alloying.

The only experimental data available for this system are from Kuz'ma et al. [45] and Zakharov et al. [46]. Kuz'ma et al. [45] presented an isothermal section at 1,400°C. As Figure 22 shows, the present calculations agree well with their experimental

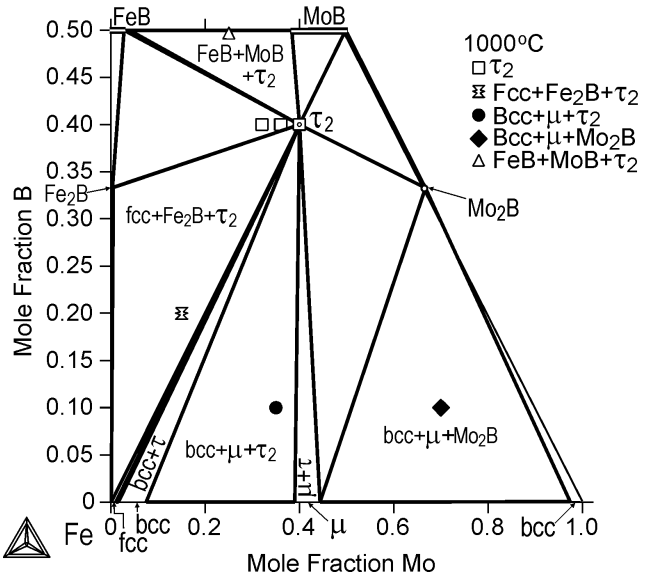

Fig. 18. Calculated isotherm of 1,000°C in the Fe-B-Mo system, with experimental data points of Gladyshevskii et al. [44]

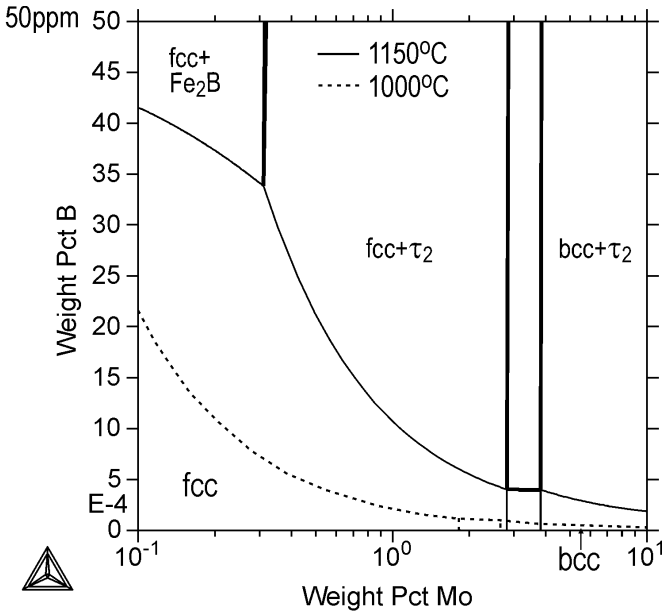

Fig. 19. Calculated solubility of B in the fcc and bcc phases of the Fe-B-Mo system at 1,150 and 1,000°C

data. Note, however, the two-phase symbols inside the calculated three-phase triangle of Cr_5B_3-Mo_2B-MoB. These symbols refer to the two phase region of CrB-Mo_2B detected by [45]. Neither could Tojo et al. [27] reconstruct that two-phase region in their calculations. The calculations by Tojo et al. [27] suggest that the Cr solubility in the Mo-B side Mo_2B phase is higher than calculated in this work, which gives better agreement with the measured [45] one-phase symbol at 58 at% Mo and 33.3 at% B. At the same time, however, the neighboring two-phase symbols [45] are clearly located in their calculated three-phase region of Cr_5B_3-Mo_2B-bcc, whereas only one of these symbols (at 55 at% Mo and 31 at% B) is located in that same region calculated in this work. On the whole, it seems impossible to reconstruct all the phase equilibria reported by Kuz'ma et al. [45], unless one does not apply extremely complex composition dependencies for the interaction parameters of the borides.

The three calculated isotherms of 1,800°C (Fig. 21), 1,400°C (Fig. 22), and 1,000°C (Fig. 23) show that in this system, the temperature does not greatly influence the solid-state phase-equilibria. The M_3B_2 boride remains stable in the middle of the diagrams, agreeing with the calculations of Tojo et al. [27]. Nevertheless, first measurements for the liquid phase or the liquidus surfaces of this system will doubtless lead to a new evaluation of the most boride expressions.

Zakharov et al. [46] presented a vertical section of $w_B = w_{Cr}$ in the Mo-rich part of the system, as shown in Figure 24. The

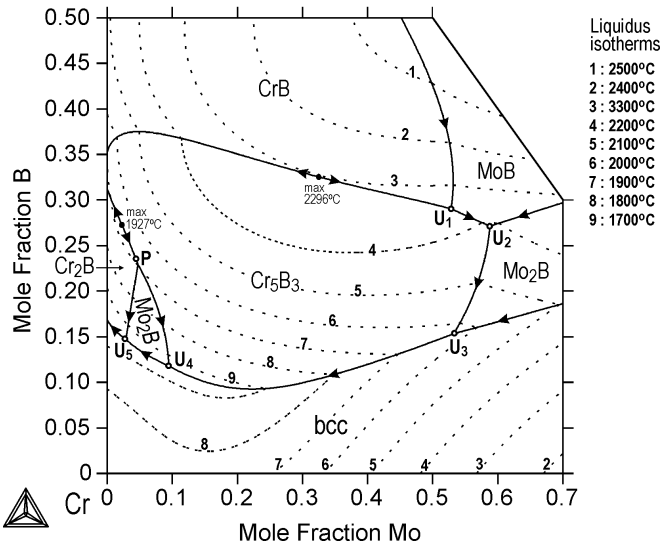

Fig. 20. Calculated liquidus projection of the B-Cr-Mo system. The calculated liquidus isotherms between 2,500 and 1,700°C are also shown (dotted lines)

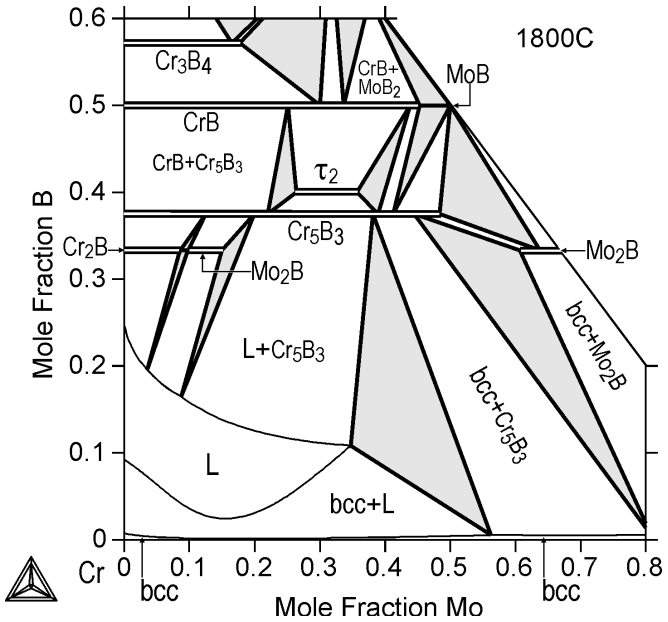

Fig. 21. Calculated isotherm of 1,800°C in the B-Cr-Mo system. Calculated three-phase triangles are shown in gray

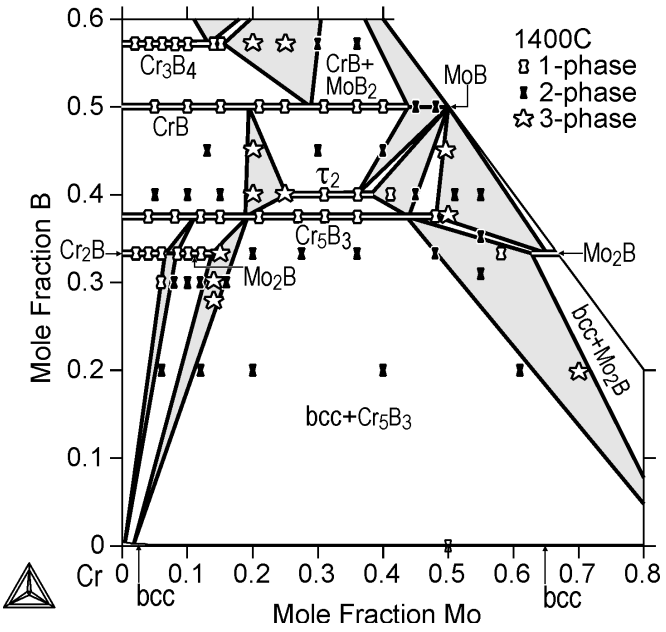

Fig. 22. Calculated isotherm of 1,400°C in the B-Cr-Mo system, with experimental data points of Kuz'ma et al. [45]. Calculated three-phase triangles are shown in gray

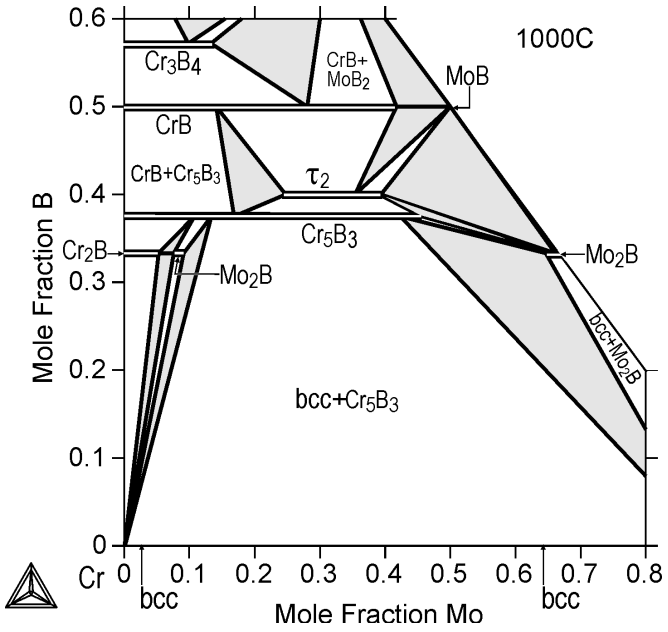

Fig. 23. Calculated isotherm of 1,000°C in the B-Cr-Mo system. Calculated three-phase triangles are shown in gray

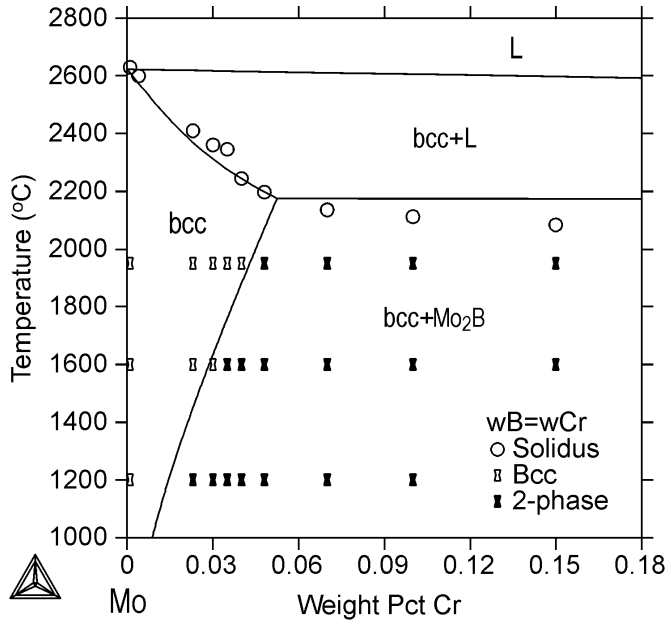

Fig. 24. The calculated vertical section of $w_B = w_{Cr}$ in the Mo-rich part of the Cr-Mo-B system, with experimental data points by Zakharov et al. [46]. Term w_i denotes the weight fraction of solute i

present calculations agree well with these measurements when applying the earlier optimized B-Mo interaction parameter of the bcc phase (Table 3) in the calculations.

3.4. System Fe-B-Cr-Mo

The given parameters were optimized using the measurements of Kim et al. [47] and Baliga [48] for three Fe-Cr-B-Mo alloys at 1,000°C. The results of the calculations are presented in Tables 8 and 9, showing reasonable agreement with the experimental data.

4. Conclusions

The previously mentioned study of the development of the Iron Alloy Database (IAD) has been continued by treating boron as a substitutional element in the bcc and fcc phases of steels. The present study introduces a thermodynamic description for the ternary Fe-B-Mo system and its extension to the quaternary

TABLE 6

Calculated invariant points in the B-Cr-Mo system

Reaction	Type	T (°C)	at % Mo in liquid	at % B in liquid
$L + CrB = Cr_5B_3 + MoB$	U_1	2,236	52.82	29.05
$L + MoB = Cr_5B_3 + Mo_2B$	U_2	2,190	58.78	27.13
$L + Mo_2B = bcc + Cr_5B_3$	U_3	1,968	53.24	15.34
$L + Cr_5B_3 = bcc + Mo_2B$	U_4	1,661	9.46	11.79
$L + Mo_2B = bcc + Cr_2B$	U_5	1,646	2.84	14.69
$L + Cr_2B + Cr_5B_3 = Mo_2B$	P	1,901	4.69	22.92

TABLE 7

Calculated enthalpies (kJ/mol) of formation of borides CrB, Cr_3B_4, and M_3B_2 in the B-Cr-Mo system with different site fractions of Mo (y_{Mo}), and those obtained by the first-principle calculations (FPC) of Tojo et al. [27]

	y_{Mo} = 0.333		y_{Mo} = 0.500		y_{Mo} = 0.667		y_{Mo} = 1	
Boride	Calc.	FPC	Calc.	FPC	Calc.	FPC	Calc.	FPC
CrB	–44.4	–45.6	–46.2	–44.5	–47.9	–45.8	–50.7	–50.6
Cr_3B_4	–44.7	–41.6	–44.5	–40.4	–43.4	–39.3	–39.0	–39.8
M_3B_2	–44.4	–44.3	–48.9	–44.1	–51.4	–45.9	–	–39.1

TABLE 8

Calculated phase fractions and compositions in the Fe-18at%Cr-2at%Mo-10at%B (Fe-18.2wt%Cr-3.73wt%Mo-2.1wt%B) alloy at 1,000°C, with experimental phase compositions of Kim et al. [47]

Phase	Phase fraction	at % Fe	at % Cr	at % Mo	at % B	Reference
fcc	0.713	89.14	10.60	0.26	0.004	Calc. This study
	0.715	90.0	9.8	0.07	0.006	Calc. [24]
		87.0	12.0	1.00	0	Exp. [46]
Cr_2B	0.221	23.68	41.96	1.03	33.33	Calc. This study
	0.212	20.3	44.8	1.54	33.3	Calc. [24]
		31.0	34.7	1.00	33.3	Exp. [46]
M_3B_2	0.065	17.89	17.84	24.27	40.0	Calc. This study
	0.073	18.4	19.4	22.2	40.0	Calc. [24]
		16.8	19.2	24.0	40.0	Exp. [46]

TABLE 9

Calculated atomic ratios of the metallic elements in two Fe-Cr-Mo-B alloys at 1,000°C, with experimental ratios of Baliga [48]

Alloy	**Fcc** **Fe : Cr : Mo**	**Cr_2B** **Fe : Cr : Mo**	**M_3B_2** **Fe : Cr : Mo**	
A	90.51 : 9.27 : 0.22 87.0 : 12.0 : 1.00	36.41 : 62.28 : 1.31 45.2 : 53.3 : 1.50	30.53: 30.36 : 39.11 29.0 : 33.0 : 38.0	Calc. Exp.
B	88.73 : 11.00 : 0.27 85.5 : 13.9 : 0.60	35.27 : 63.13 : 1.60 45.0 : 53.6 : 1.40	29.59 : 29.59 : 40.82 29.0 : 30.0 : 41.0	Calc. Exp.

Alloys: A = 16.6wt%Cr-3.79wt%Mo-2.03wt%B, B = 19.2wt%Cr-3.42wt%Mo-2.18wt%B

Fe-B-Cr-Mo system by also assessing the binary B-Mo and the ternary Cr-Mo-B systems. The descriptions of the other binary and ternary systems, i.e. Fe-B, Fe-Cr, Fe-Mo, Cr-B, Cr-Mo, Fe-B-Cr, and Fe-Cr-Mo, were retained from already published sources. In the current Fe-B-Cr-Mo description, 24 phases (liquid, bcc, fcc, Chi, Mu, R, Sigma, Fe_2Mo, Fe_2B, FeB, Cr_2B, Cr_5B_3, CrB, Cr_3B_4, CrB_2, CrB_4, Mo_2B, MoB, MoB_2, Mo_2B_5, MoB_4, $Fe_{14}MoB_5$, M_3B_2, and beta-rhombo-B) have been considered. Experimental thermodynamic and phase equilibrium data have been used for the optimization of the B-Mo, Fe-B-Mo, Cr-Mo-B, and Fe-B-Cr-Mo systems. A good agreement was obtained between the calculated and the experimental thermodynamic and phase equilibrium data.

Acknowledgement

This study was executed within the framework of the Genome of Steel profiling project. The Academy of Finland (project 311934) is acknowledged for funding this study.

REFERENCES

[1] J. Miettinen, G. Vassilev, Arch. Metall. Mater. **59** (2), 601-607 (2014).

[2] J. Miettinen, G. Vassilev, Arch. Metall. Mater. **59** (2), 609-614 (2014).

[3] J. Miettinen, K. Lilova, G. Vassilev, Arch. Metall. Mater. **59** (4), 1481-1485 (2014).

[4] J. Miettinen, V.-V. Visuri, T. Fabritius, N. Milcheva, G. Vassilev, Arch. Metall. Mater. **64** (2), 451-456 (2019).

[5] J. Miettinen, V.-V. Visuri, T. Fabritius, N. Milcheva, G. Vassilev, Arch. Metall. Mater. **64** (4), 1239-1248 (2019).

[6] J. Miettinen, V.-V. Visuri, T. Fabritius, N. Milcheva, G. Vassilev, Arch. Metall. Mater. **64** (4), 1249-1255 (2019).

[7] J. Miettinen, V.-V. Visuri, T. Fabritius, G. Vassilev, Arch. Metall. Mater. **65** (2), 923-933 (2020).

[8] J. Miettinen, V.-V. Visuri, T. Fabritius, Acta Univ. Oul. C, 704 (2019).

[9] J. Miettinen, S. Louhenkilpi, H. Kytönen, J. Laine, Math. Comput. Simulat. **80** (7), 1536-1550 (2010).

[10] J. Miettinen, S. Louhenkilpi, V.-V. Visuri, T. Fabritius, IOP Conf. Ser. Mater. Sci. Eng. **529**, article 012063 (2019).
[11] B. Hallemans, P. Wollants, J. R. Roos, Z. Metallkd. **85** (10), 676-682 (1994).
[12] J.-O. Andersson, B. Sundman, Calphad **11** (1), 83-92 (1987).
[13] B.-J. Lee, Calphad **17** (3), 251-268 (1993).
[14] J.-O. Andersson, Calphad **12** (1), 9-23 (1988).
[15] J. Miettinen, A. Pashkova, G. Vassilev, J. Phase Equilb. Diff. **36** (3), 60-67 (2014).
[16] J. Miettinen, V.-V. Visuri, T. Fabritius, Acta Univ. Oul. C, 758 (2020).
[17] C.E. Campbell, U.R. Kattner, Calphad **26** (3), 477-490 (2002).
[18] J.-O. Andersson, N. Lange, Metall. Trans. A **19** (6), 1385-1394 (1988).
[19] K.E. Spear, M.S. Wang, Calphad **5** (2), 109-113 (1981).
[20] Y. Yang, Y.A. Chang, Intermetallics **13** (2), 121-128 (2005).
[21] K. Yamada, H. Ohtani, M. Hasebe, J. Japan Inst. Met. **73** (3), 180-188 (2009).
[22] V.T. Vitusiewicz, A.A. Bondar, U. Hecht, O.A. Potazhevska, Y.Ya. Velikanova, J. Alloys and Compounds **655**, 336-352 (2016).
[23] X.O. Yang, F. Yin, J. Hu, M. Zhao, Y. Liu, Calphad **59**, 189-198 (2017).
[24] L.-M. Pan, Phase equilibria and elastic moduli of rapidly solidified Fe-Cr-B-Mo and Fe-Cr-Ni-B alloys, Doctoral Thesis, University of Surrey, Guildford, United Kingdom, 1992.
[25] H. Haschke, H. Nowotny, F. Benesovsky, Monatsch Chem. **97**, 1459-1468 (1966).
[26] A. Leithe-Jasper, H. Klesnar, P. Rogl, M. Komai, K.I. Takagi, Nippon Kinzoku Gakkai-Shi **64** (2), 154-162 (2000).
[27] M. Tojo, T. Tokunaga, H. Ohtani, M. Hasebe, Calphad **34** (3), 263-270 (2010).
[28] H. Lukas, S.G. Fries, B. Sundman, Computational Thermodynamics: The Calphad Method, Cambridge University Press, Cambridge, United Kingdom (2007).
[29] E. Rudy, S. Windisch, USAF Tech. Report AFML-TR-65-2, Part V, Wright Patterson Air Force Base, OH, USA, 1969.
[30] E. Storms, B. Müller, J. Phys. Chem. **81** (4), 318-324 (1977).
[31] L. Brewer, R.H. Lamoreaux, II. Phase Diagrams, Molybdenum: Physico-chemical properties of its compounds and alloys, Special Issue No. 7, International Atomic Energy Agency, Vienna, Austria, 1980, pp. 193-365.
[32] Y.-C. Chuang, T.-L. Chuang, C.-H. Wu, Sci. Sinica, Peking **13**, 1851 (1964).
[33] V. I. Kharitonov, M.S. Makunin, F.I. Shamray, Russ. Metall. (3), 113-116 (1971).
[34] A.M. Zakharov, I.L. Novikov, V.C. Polkin, Izv. Vyssh. Uchebn. Zaved. Tsvetn. Met. **14**, 126-129 (1971).
[35] M. Morishita, K. Koyama, S. Yagi, G. Zhang, J. Alloys Compd. **314**, 212-218. (2001).
[36] P. Franke, D. Neuschütz, B2, B-Mo, Binary Systems. Part 2: Elements and Binary Systems from B-C to Cr-Zr, IV Phys. Chem., vol. 19, Springer-Verlag, 2004, pp. 1-4.
[37] V.M. Maslov, A.S. Neganov, I.P. Borovinskaya, A.G. Merzhanov, Akad. Nauk. SSSR Fiz. Goren. Vzryva **14** (6), 73-82 (1978).
[38] E.G. Lavut, M.V. Chelovskaya, O.E. Kashireninov, J. Eng. Phys. Thermophys. **65** (4), 971-973 (1993).
[39] F. Baehren, D. Vollath, Planseeber. Pulvermet. **17** (3), 180-183 (1969).
[40] S. Omori, Y. Hashimoto, K. Koyama, J. Jpn. Inst. Met. **45**, 1107-1111 (1981)
[41] S. Omori, Y. Hashimoto, K. Koyama, Kouon Gakkai-shi **7** (5), 204-208 (1981).
[42] M.I. Serbova, "Investigation of Thermodynamic Properties of Borides of Transition Metals in High-temperature Range" (in Russian), Ph.D. thesis, Frantsevich Institute for Problems of Materials Science, Kyiv, Ukraine, 1982, p. 174.
[43] A.S. Bolgar, A.V. Blinder, M.I. Serbova, Powder Metall. Met. Ceram. **29** (12), 977-981 (1990).
[44] E.I. Gladyshevskii, T.F. Fedorov, Y.B. Kuz'ma, R. V. Skolozdra, Sov. Powder Metall. Ceram. **5** (4), 305-309 (1966).
[45] Y.B. Kuz'ma, V.S. Telegus, D.A. Kovalyk, Sov. Powder Metall. Met. Ceram. **8** (5), 403-410 (1969).
[46] A.M. Zakharov, S.I. Yudkovskii, Y.S. Popova, Inorganic Materials **18** (10), 1472-1474 (1982).
[47] W.T. Kim, B. Cantor, K. Clay, C. Small, In-situ particulate composites manufactured by hot extrusion of a melt spun amorphous Fe70-Cr18-Mo2-B18 alloy, in: Fundamental Relationships between Microstructure and Mechanical Properties of Metal Matrix Composites, P.K. Liaw and M.N. Gungor, eds., TMS-AIME, Warrendale, 1990, p.89
[48] C. Baliga, Results from the renewed contract with Rolls-Royce plc,1989-1991, University of Surrey, UK, 1991.
[49] A.T. Dinsdale, SGTE unary database, version 4.4.
[50] I. Ansara, A.T. Dinsdale, M.H. Rand, COST 507 - Thermochemical database for light metal alloys, Volume 2, European Communities, Belgium, 1998.
[51] J.-O. Andersson, T. Helander, L. Höglund, P. Shi, B. Sundman, Calphad **26** (2), 273-312 (2002).
[52] T. Ide, T. Ando, Metall. Trans. A **20** (1), 17-24 (1989).
[53] V. Raghavan, J. Phase Equilib. **24** (5), 449-450 (2003).